Gridless Azimuth and Polarization Parameter Estimation Based on Uniform Circular COLD Arrays

Tao YU, Lutao LIU

College of Information and Communication Engineering, Harbin Engineering University, Harbin, 150001, China

yutao_hi@hrbeu.edu.cn, liulutao@hrbeu.edu.cn

Submitted November 11, 2024 / Accepted January 6, 2025 / Online first March 18, 2025

Abstract. *In order to achieve gridless azimuth and polarization parameter estimation, the polarization atomic norm minimization (P-ANM) algorithm is proposed. The polarization-sensitive uniform circular array (P-UCA) consisting of concentered orthogonal loop and dipole (COLD) antennas is considered in this paper for its stable estimation ability for all* $0^\circ \sim 360^\circ$ *range. The proposed method is capable of estimating the parameters with only single snapshot and overcomes the grid mismatch. First, the the mathematical models of signals received by the P-UCA are established and the P-ANM algorithm is applied. Then, The P-UCA is mapped into the virtual uniform linear array based on the Fourier expansion. Subsequently, the dual method is employed to solve the P-ANM model and determine the azimuths of the signals. Ultimately, by reconstructing the signal vectors, the polarization information can be inversely estimated based on the relationship between the electrical and magnetic signals. The simulations demonstrate that the proposed P-ANM algorithm exhibits superior joint estimation ability for all the azimuth and polarization parameters of the signals.*

Keywords

Polarization Sensitive Array (PSA), Uniform Circular Array (UCA), Concentered Orthogonal Loop and Dipole (COLD), Atomic Norm Minimization (ANM)

1. Introduction

Polarization is an important attribute of electromagnetic waves, along with amplitude and phase. The utilization of polarization information in array systems has been demonstrated to markedly enhance the operating performance, including robust detection capabilities and outstanding immunity to interference [1]. Since the polarization sensitive array (PSA) employs electromagnetic vector sensors (EMVS) instead of conventional scalar sensors, it can simultaneously sense the polarization and spatial information of the signals, and then demonstrate superior identifying and tracking abilities. Nowadays, the PSA plays an important role in various industries, including radar detection [2], [3], aeronautics [4], remote sensing [5], and others.

Signal parameter estimation is a crucial task for the PSA, especially for the direction and polarization information. Extensive research has been conducted on this topic by scholars [6–9]. As with scalar array signal processing, the traditional approach is to use spatial spectrum estimation techniques, such as the polarization Multiple Signal Classification (P-MUSIC) algorithm and the polarization Estimating Signal Parameter via Rotational Invariance Techniques (P-ESPRIT) algorithm. Based on the quaternion theory, the quaternion-MUSIC (Q-MUSIC) [10] algorithm, the biquaternion-MUSIC (BQ-MUSIC) [11] algorithm were proposed to deal with the polarization information. For the ESPRIT method, the quaternion-ESPRIT (Q-ESPRIT) [12] algorithm is also existing. The problem with the quaternion method is the limited improvement in estimation performance compared with the P-MUSIC and P-ESPRIT. Until now, the spectrum-based methods are still popular. In [13], the augmented tensor-MUSIC (AT-MUSIC) was proposed by expressing the signal models of the nested arrays as tensors. And in [14], the augmented nested quaternion-MUSIC (ANQ-MUSIC) was proposed by vectorizing the quaternion covariance matrix of the difference co-arrays. The augmented quaternion ESPRIT (AQ-ESPRIT) [15] was also proposed to deal with the co-located crossed-dipole arrays.

However, the spectrum-based methods require a considerable number of snapshots to construct the covariance matrices. The methods based on signal sparse representation bring the possibility for parameter estimation with only single snapshot [16–18]. In recent years, it was introduced to the PSA field. In [19], the parameters of the cross-dipole arrays were estimated using weighted group lasso formulation and an unbiased estimator was obtained. In [20], the sparse-based algorithm was considered to deal with the situation where there exist both time-varying and stationary parameters. And in [21], the author used block-sparsity reconstruction for estimation with unknown source numbers. In [22], the coherence signal parameters were estimated, which is often the case in underwater situations.

DOI: 10.13164/re.2025.0109

The atomic norm minimization (ANM) algorithm [23], also known as the gridless parameter estimation method, is attracting much attention because it can overcome the grid mismatch caused by traditional sparse-based methods. It was first analysed in detail for direction estimation in [24]. Later, some more complex situations were discussed. By vectoring the data matrices of the planar arrays, the two-dimensional ANM algorithm was proposed [25]. And by matrix interpolation, the parameter estimation of coprime arrays was solved by ANM algorithm. Later, the signals with phase-gain errors [26], [27] and the non-circular signals [28] were also considered. However, the research was limited to the line array situation, and there was little focus on the PSA parameter estimation.

Since the uniform circular array (UCA) has the excellent property of isotropy [29] and the concentered orthogonal loop and dipole (COLD) antennas have the simple signal models [30], this paper investigates the parameter estimation of the polarization-sensitive UCA (P-UCA) composed of the COLD antennas. First, the polarization ANM (P-ANM) formulation is established. And then we convert the signals received from the P-UCA into those received from the virtual uniform line arrays, so that the P-ANM can deal with. We solve the P-ANM by its dual problem and obtain the gridless azimuth parameters by polynomial rooting. Finally, by the retrieval of the signal vectors, the polarization parameters are obtained by analyzing the connections of the signals received by the loops and dipoles.

The rest of the papers is organized as follows: Section 2 gives the mathematic model of the P-UCA. Section 3 proposes the gridless P-ANM algorithm and its solving method. Section 4 verifies the P-ANM algorithm by simulations. Section 5 concludes the paper.

Notations used in this paper are as follows: $(\mathbf{A})^{\mathrm{T}}$, $(\mathbf{A})^{\mathrm{H}}$ and $(\mathbf{A})^{\dagger}$ denote the transpose, conjugate transpose and pseudo-inverse of the matrix $\mathbf{A}$. $\mathbf{A} \geq 0$ denotes that the matrix $\mathbf{A}$ is positive semidefinite (PSD). $\|\mathbf{a}\|_{\infty}$ denotes the infinity norm of the vector $\mathbf{a}$. $|\bullet|$ denotes the modulus of the complex values, $\mathrm{Re}\,(\bullet)$ denotes the extraction of the real part, and $\arg(\bullet)$ denotes the extraction of the phase. $(\bullet)^*$ denotes the conjugate of the complex values. $\hat{a}$ denotes the estimation of variable a.

2. The Signal Model of the P-UCA

As shown in Fig.1, in this paper we consider a P-UCA with M EMVS equally spaced around the entire circumference. All the EMVS use the COLD antennas and all the magnetic loops are placed in the $x-y$ plane. Then the electric dipoles are parallel to the $z-$axis. As in regular circular array model, we use polar coordinates to express the location of each EMVS. The location of the mth EMVS is (p, ξ_m), where p is the radius and ξ_m is the polar angle by setting x-axis as the reference direction.

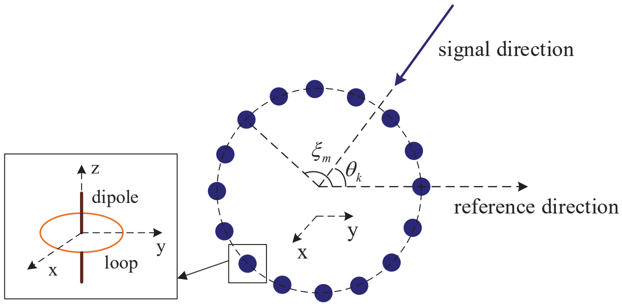

Fig. 1. The arrangement of the P-UCA.

Suppose there are K narrowband and far-field signals of frequency f (wavelength λ) incident on the P-UCA. The azimuth of the kth signal is $\theta_k \in (0, 2\pi]$. Then the spatial response of the mth EMVS can be expressed as

$$\begin{aligned} u_m(\theta_k) &= \mathrm{e}^{-\mathrm{j}2\pi f \tau_m(\theta_k)} \\ &= \mathrm{e}^{-\mathrm{j}2\pi p \cos(\theta_k - \xi_m)/\lambda}, \quad m = 1, \cdots, M \end{aligned} \tag{1}$$

where $\tau_m(\theta_k)$ is the propagation delay with respect to the origin. Then the spatial steering vector of the kth signal is

$$\begin{aligned} \mathbf{u}(\theta_k) &= [u_1(\theta_k), u_2(\theta_k), \cdots, u_M(\theta_k)]^{\mathrm{T}} \\ &= \mathrm{e}^{-\mathrm{j}2\pi p \cos(\theta_k - \xi)/\lambda} \end{aligned} \tag{2}$$

where $\xi = [\xi_1, \xi_2, \cdots, \xi_M]^{\mathrm{T}}$ is the vector contains the polar angles of all the EMVS.

Due to the central symmetry of the COLD antennas, they are highly suitable for use in circular arrays. A COLD antenna pair consists of an orthogonal electric dipole and a magnetic loop, with the dipole passing through the center of the loop. The dipole is used to receive the electric field component of the signals, and the loop is used to receive the magnetic field component [31], [32]. According to the polarization theory of electromagnetic waves [33], suppose the signals are fully polarized and the polarization parameters of the kth signal is (γ_k, η_k), where $\gamma_k \in (0, \pi/2]$ is the polarization angle and $\eta_k \in (0, 2\pi]$ is the polarization phase difference, the polarization vector of the kth signal can be expressed as [34], [35]

$$\mathbf{p}_k = \begin{bmatrix} p_k^{[\mathrm{e}]} \\ p_k^{[\mathrm{h}]} \end{bmatrix} = \begin{bmatrix} -\sin\gamma_k \mathrm{e}^{\mathrm{j}\eta_k} \\ -\cos\gamma_k \end{bmatrix}. \tag{3}$$

Simultaneously influenced by the spatial and polarization parameters, the final signals received by the electric dipoles and the magnetic loops can be expressed respectively as

$$\begin{aligned}\mathbf{x}_\mathrm{e} &= \sum_{k=1}^{K} p_k^{[\mathrm{e}]}\mathbf{u}\left(\theta_k\right)s_k\\ &= \sum_{k=1}^{K} -\sin\gamma_k \mathrm{e}^{\mathrm{j}\eta_k}\mathrm{e}^{-\mathrm{j}2\pi p\cos(\theta_k-\xi)/\lambda}s_k,\\ \mathbf{x}_\mathrm{h} &= \sum_{k=1}^{K} p_k^{[\mathrm{h}]}\mathbf{u}\left(\theta_k\right)s_k\\ &= \sum_{k=1}^{K} -\cos\gamma_k \mathrm{e}^{-\mathrm{j}2\pi p\cos(\theta_k-\xi)/\lambda}s_k\end{aligned} \tag{4}$$

where s_k is the complex amplitude of the kth signal. In the next processing, the polarization parameters have no effect on solving azimuth parameters, so they are first absorbed into the signal s_k as

$$\begin{aligned}\mathbf{x}_\mathrm{e} &= \sum_{k=1}^{K}\mathbf{u}\left(\theta_k\right)s_{\mathrm{e}k} = \mathbf{U}\left(\theta\right)\mathbf{s}_\mathrm{e},\\ \mathbf{x}_\mathrm{h} &= \sum_{k=1}^{K}\mathbf{u}\left(\theta_k\right)s_{\mathrm{h}k} = \mathbf{U}\left(\theta\right)\mathbf{s}_\mathrm{h}\end{aligned} \tag{5}$$

where $\mathbf{s}_\mathrm{e}$ and $\mathbf{s}_\mathrm{h}$ are the pseudo signal vectors containing the polarization information, $\theta = [\theta_1, \cdots \theta_K]$ is the vector, and $\mathbf{U}\left(\theta\right) = \left[\mathbf{u}\left(\theta_1\right), \mathbf{u}\left(\theta_2\right), \cdots, \mathbf{u}\left(\theta_K\right)\right]$ is the manifold matrix only containing the azimuth information.

3. The Proposed P-ANM Algorithm

3.1 Traditional On-grid Algorithm

Based on (5), if using traditional on-grid methods to estimate the azimuth parameter, we can first divide the parameter domain into a series of grids with the total number of R. The azimuth corresponding to the rth grid is θ_r , and we can construct the steering vector $\tilde{\mathbf{u}}\left(\theta_r\right)$ and the manifold matrix $\tilde{\mathbf{U}}\left(\theta\right) = \left[\tilde{\mathbf{u}}\left(\theta_1\right), \tilde{\mathbf{u}}\left(\theta_2\right), \cdots, \tilde{\mathbf{u}}\left(\theta_R\right)\right]$. Then the signals $\mathbf{x}_\mathrm{e}$ and $\mathbf{x}_\mathrm{h}$ can be given as

$$\begin{aligned}\mathbf{x}_\mathrm{e} &= \sum_{r=1}^{R}\tilde{\mathbf{u}}\left(\theta_r\right)\tilde{s}_{\mathrm{e}r} = \tilde{\mathbf{U}}\left(\theta\right)\tilde{\mathbf{s}}_\mathrm{e},\\ \mathbf{x}_\mathrm{h} &= \sum_{r=1}^{R}\tilde{\mathbf{u}}\left(\theta_r\right)\tilde{s}_{\mathrm{h}r} = \tilde{\mathbf{U}}\left(\theta\right)\tilde{\mathbf{s}}_\mathrm{h}\end{aligned} \tag{6}$$

where $\tilde{\mathbf{s}}_\mathrm{e}$ and $\tilde{\mathbf{s}}_\mathrm{h}$ are corresponding gridded pseudo signal vectors, and any $\tilde{s}_{\mathrm{e}r}$ and $\tilde{s}_{\mathrm{h}r}$ denote the imaginary energy on the rth grid. If there exist signals on corresponding grids the $\tilde{s}_{\mathrm{e}r}$ and $\tilde{s}_{\mathrm{h}r}$ are non-zero, or their values are zero. In general, the grid number is much larger than the signal number, so most of them are zero. According to the sparse representation theory [36], we can estimate the parameter by minimizing the polarization l_1 norm:

$$\begin{aligned}&\min_{\tilde{s}_{\mathrm{e}r}} \sum_{r=1}^{R}\left|\tilde{s}_{\mathrm{e}r}\right| \quad \text{s.t. } \mathbf{x}_\mathrm{e} = \sum_{r=1}^{R}\tilde{\mathbf{u}}\left(\theta_r\right)\tilde{s}_{\mathrm{e}r},\\ &\min_{\tilde{s}_{\mathrm{h}r}} \sum_{r=1}^{R}\left|\tilde{s}_{\mathrm{h}r}\right| \quad \text{s.t. } \mathbf{x}_\mathrm{h} = \sum_{r=1}^{R}\tilde{\mathbf{u}}\left(\theta_r\right)\tilde{s}_{\mathrm{h}r}.\end{aligned} \tag{7}$$

The optimization problem is convex and can be easily solved by many optimization tools. The aim is to reconstruct $\tilde{\mathbf{s}}_\mathrm{e}$ and $\tilde{\mathbf{s}}_\mathrm{h}$, and the azimuths corresponding to the locations where the values are non-zero are the estimation results. Obviously, if the real signals do not lie on the grids, there will be errors in the estimation results.

3.2 The P-ANM Model and its Dual Solution

In order to estimate the gridless parameters, the l_1 norm of the pseudo signals $\mathbf{s}_\mathrm{e}$ and $\mathbf{s}_\mathrm{h}$ are minimized directly as [37]

$$\begin{aligned}\left\|\mathbf{x}_\mathrm{e}\right\|_{\mathcal{A}} &= \min_{\theta_k}\left\{\sum_k\left|s_{\mathrm{e}k}\right| : \mathbf{x}_\mathrm{e} = \sum_k\mathbf{u}\left(\theta_k\right)s_{\mathrm{e}k}\right\},\\ \left\|\mathbf{x}_\mathrm{h}\right\|_{\mathcal{A}} &= \min_{\theta_k}\left\{\sum_k\left|s_{\mathrm{h}k}\right| : \mathbf{x}_\mathrm{h} = \sum_k\mathbf{u}\left(\theta_k\right)s_{\mathrm{h}k}\right\}\end{aligned} \tag{8}$$

which are called the polarization atomic norm of the dipoles and the loops, respectively. And the method is called P-ANM algorithm. Different from (7), The grids are not divided in the azimuth domain. The $\mathbf{U}\left(\theta\right)$ is seen as the unknown parameter for solving the problem, and the aim is exactly to recover the optimal atomic set $\mathbf{U}\left(\hat{\theta}\right) = \left[\mathbf{u}\left(\hat{\theta}_1\right), \cdots, \mathbf{u}\left(\hat{\theta}_K\right)\right]$. Since every $\hat{\theta}_k$ in the $\mathbf{u}\left(\hat{\theta}_k\right)$ can take continuous values, the P-ANM algorithm overcomes the grid mismatch. However, the problems are difficult to calculate directly. Instead, we use their dual problems expressed as [38]

$$\begin{aligned}&\max_{\mathbf{c}_\mathrm{e}} \quad \mathrm{Re}\left({\mathbf{c}_\mathrm{e}}^\mathrm{H}\mathbf{x}_\mathrm{e}\right) \quad \text{s.t.} \quad \left\|\mathbf{U}(\theta)^\mathrm{H}\mathbf{c}_\mathrm{e}\right\|_\infty \le 1,\\ &\max_{\mathbf{c}_\mathrm{h}} \quad \mathrm{Re}\left({\mathbf{c}_\mathrm{h}}^\mathrm{H}\mathbf{x}_\mathrm{h}\right) \quad \text{s.t.} \quad \left\|\mathbf{U}(\theta)^\mathrm{H}\mathbf{c}_\mathrm{h}\right\|_\infty \le 1\end{aligned} \tag{9}$$

where $\mathbf{c}_\mathrm{e}$ and $\mathbf{c}_\mathrm{h}$ are the dual variables. Furthermore, each of (9) can be converted to a solvable SDP problem

$$\begin{aligned}&\max_{\mathbf{c}} \quad \mathrm{Re}\left(\mathbf{c}^\mathrm{H}\mathbf{x}\right)\\ &\text{s.t.} \quad \begin{bmatrix}\mathbf{Q}_{M\times M} & \mathbf{c}_{M\times 1}\\ \mathbf{c}^\mathrm{H} & 1\end{bmatrix} \ge 0\\ &\qquad \sum_{i=1}^{M-j}\mathbf{Q}_{i,i+j} = \begin{cases}1, & j=0\\ 0, & j=1,\cdots,M-1\end{cases}\end{aligned} \tag{10}$$

where $\mathbf{c}$ denotes either $\mathbf{c}_\mathrm{e}$ or $\mathbf{c}_\mathrm{h}$, $\mathbf{x}$ denotes corresponding $\mathbf{x}_\mathrm{e}$ or $\mathbf{x}_\mathrm{h}$. And from the detail of getting (9), we know the θ solution of $\left|\mathbf{U}(\theta)^\mathrm{H}\mathbf{c}\right| = 1$ corresponds to the true azimuth estimation. If $\hat{\mathbf{c}}$ is obtained from (10), and the array is uniform of element space, $\mathbf{u}\left(\hat{\theta}_k\right)$ can be then obtained by polynomial rooting of the trigonometric polynomial

$$P\left(\mathbf{z}\right) = 1 - \left|\mathbf{U}(\theta)^\mathrm{H}\mathbf{c}\right|^2 = 1 - \sum_{m=-(M-1)}^{M-1} r_m\mathbf{z}^m \tag{11}$$

where $\mathbf{z} = \exp\left(-\mathrm{j}\pi\sin\theta\right)$. The coefficients $r_m = \sum_{l=0}^{M-1-m} c_l c_{l+m}^*, m \ge 0$ and $r_{-m} = r_m^*$, are the autocorrelation of $\hat{\mathbf{c}}$. Unfortunately, the P-UCA is not a kind of uniform arrays for the delay between any two adjacent COLD antenna pairs are not constant. It makes it impossible to directly use the polynomial rooting method to solve $\mathbf{z}$. Further processing is necessary.

3.3 Virtual Mapping of the Steering Vectors

In this paper, we transform the steering vectors of the P-UCA to the Fourier domain to solve the non-uniform situation. Define the function $b(\theta) = \mathbf{U}(\theta)^{\mathrm{H}}\mathbf{c}$, where the variable θ is regarded as a continuous variation. And then perform the Fourier expansion of $b(\theta)$, we have

$$b(\theta) = \sum_{n=-N}^{N} \sum_{m=1}^{M} (\alpha_m [n] \, c_m) \exp(\mathrm{j}n\theta) \tag{12}$$

where $\alpha_m[n]$ is the Fourier coefficients, N is the Fourier expansion term number. The $\alpha_m[n]$ can be calculated by sampling from $\mathbf{u}^*(\theta)$ with large DFT points $P = 2N+1$ as

$$\alpha_m [n] = \frac{1}{P} \sum_{l=-N}^{N} u_m^* (l\Delta\theta) \exp(-\mathrm{j}\Delta\theta l n) \tag{13}$$

where $\Delta\theta = 2\pi/P$ and $n = -N, \cdots, 0, \cdots N$. From (12), it is shown that the virtual steering vector $\exp(\mathrm{j}n\theta)$ is uniform with the distribution of n. And Equation (12) can be reformulated as

$$b(\theta) = \sum_{n=-N}^{N} B_n \exp(\mathrm{j}n\theta). \tag{14}$$

And combine all the coefficients B_n as a vector form

$$\mathbf{h} = \left[B_{-N}, B_{-(N-1)}, \cdots, B_N\right]^{\mathrm{T}} = \mathbf{G}^{\mathrm{H}}\mathbf{c}. \tag{15}$$

Note here that: 1) the Fourier expansion term number N is the truncation of Fourier coefficients $\alpha_m[n]$. If we want to retain as much energy as possible of the original signals in $b(\theta)$, N needs to reach a certain threshold. In the UCA condition, the choice of the threshold is related to p/λ and can be chosen by advance testing. Figure 2 gives the energy ratio with N for the common case of $p/\lambda = 1, 2$ and 3. We can choose N based on the figure.

2) $\mathbf{G}$ is only related to the array parameters, but independent of the signal parameters, so it can be calculated offline once the array geometry is determined.

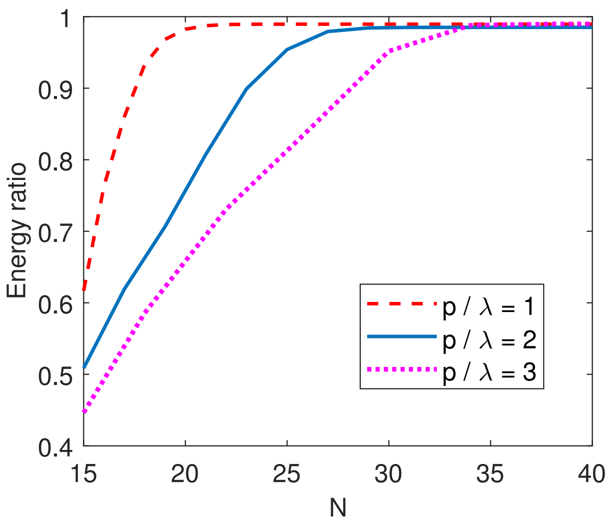

Fig. 2. The energy ratio with N.

3.4 Azimuth Estimation

After the virtual mapping, the SDP problem (10) can be converted to the new formulation corresponding to the virtual uniform array as

$$\begin{aligned} \max_{\tilde{\mathbf{c}}} \quad & \mathrm{Re}\left(\tilde{\mathbf{c}}^{\mathrm{H}}\tilde{\mathbf{x}}\right) \\ \text{s.t.} \quad & \begin{bmatrix} \tilde{\mathbf{Q}}_{P\times P} & \tilde{\mathbf{G}}^{\mathrm{H}}_{P\times 2M}\tilde{\mathbf{c}}_{2M\times 1} \\ \tilde{\mathbf{c}}^{\mathrm{H}}\tilde{\mathbf{G}} & 1 \end{bmatrix} \geq 0 \\ & \sum_{i=1}^{P-j} \mathbf{Q}_{i,i+j} = \begin{cases} 1, & j=0 \\ 0, & j = 1, \cdots, P-1 \end{cases} \end{aligned} \tag{16}$$

where $\tilde{\mathbf{x}} = [\mathbf{x}_{\mathrm{e}}; \mathbf{x}_{\mathrm{h}}]$, $\tilde{\mathbf{c}} = [\mathbf{c}_{\mathrm{e}}; \mathbf{c}_{\mathrm{h}}]$ and $\tilde{\mathbf{G}} = [\mathbf{G}, \mathbf{G}]$. Here, the two separate optimization problems in (9) are fused into one SDP problem without dimension increasing. It is easy to be solved by interior-point method. In the real situations, if the signals are contaminated by additive Gaussian white noise as

$$\begin{aligned} \mathbf{y}_{\mathrm{e}} &= \mathbf{x}_{\mathrm{e}} + \mathbf{n}_{\mathrm{e}}, \\ \mathbf{y}_{\mathrm{h}} &= \mathbf{x}_{\mathrm{h}} + \mathbf{n}_{\mathrm{h}}, \end{aligned} \tag{17}$$

the SDP problem (16) can be substituted by

$$\begin{aligned} \max_{\tilde{\mathbf{c}}} \quad & \mathrm{Re}\left(\tilde{\mathbf{c}}^{\mathrm{H}}\tilde{\mathbf{y}}\right) + \tau\|\tilde{\mathbf{c}}\|_2 \\ \text{s.t.} \quad & \begin{bmatrix} \tilde{\mathbf{Q}}_{P\times P} & \tilde{\mathbf{G}}^{\mathrm{H}}_{P\times 2M}\tilde{\mathbf{c}}_{2M\times 1} \\ \tilde{\mathbf{c}}^{\mathrm{H}}\tilde{\mathbf{G}} & 1 \end{bmatrix} \geq 0 \\ & \sum_{i=1}^{P-j} \mathbf{Q}_{i,i+j} = \begin{cases} 1, & j=0 \\ 0, & j = 1, \cdots, P-1 \end{cases} \end{aligned} \tag{18}$$

where $\tilde{\mathbf{y}} = [\mathbf{y}_{\mathrm{e}}; \mathbf{y}_{\mathrm{h}}]$ and τ is the regularization parameter to suppress the influence of noise. Our aim is to get the solution $\hat{\tilde{\mathbf{c}}}$ of the dual variable $\tilde{\mathbf{c}}$ and later $\mathbf{h} = \tilde{\mathbf{G}}^{\mathrm{H}}\hat{\tilde{\mathbf{c}}}$. As mentioned above, we then construct the dual polynomial $b(\mathbf{z}) = \sum_{n=-N}^{N} B_k \mathbf{z}^n$ with $\mathbf{z} = \exp(\mathrm{j}\theta)$. If $|b(\mathbf{z})| = 1$, the solution of $\mathbf{z}$ corresponds to the true azimuth estimation. Similarly, the nonnegative polynomial

$$H(\mathbf{z}) = 1 - |b(\mathbf{z})|^2 \tag{19}$$

is formed. Its coefficients are $r_n = \sum_{l=0}^{N-1-n} h_l h_{l+n}^*, n \geq 0$ and $r_{-n} = r_n^*$. It is easy to find the roots. Then the azimuth estimation can be recovered by locating the roots on the unit circle

$$\hat{\theta} = \arg(\hat{\mathbf{z}}), |\hat{\mathbf{z}}| = 1. \tag{20}$$

It can be shown in Fig. 3 as an example that there are three roots on the unit circle, which are the estimation results. And other roots symmetrically distributed on both sides of the unit circle.

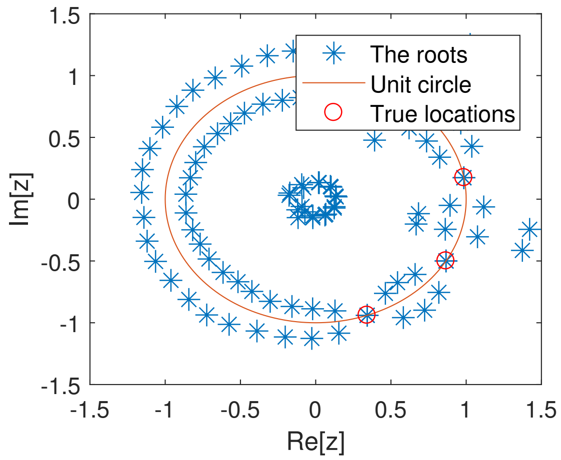

(a) The roots of $P(\mathbf{z})$

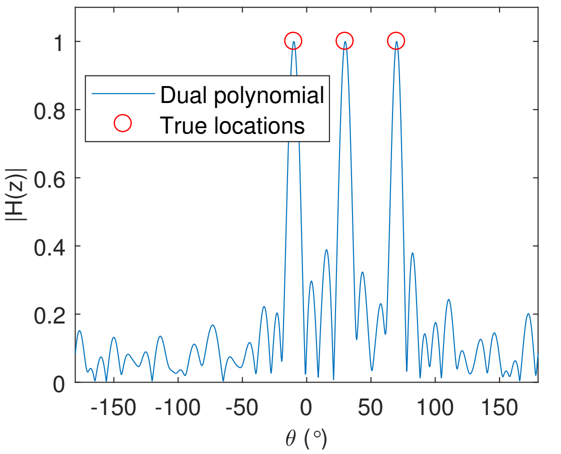

(b) The dual polynomial $H(\mathbf{z})$

Fig. 3. The display of the polynomial rooting.

3.5 Retrieval of the Polarization Parameters

If the azimuth $\hat{\theta}$ is estimated, the pseudo signal amplitudes with polarization can recovered by least squares method

$$\begin{aligned} \hat{\mathbf{s}}_{\mathrm{e}} &= \mathbf{U}\left(\hat{\theta}\right)^{\dagger}\mathbf{y}_{\mathrm{e}}, \\ \hat{\mathbf{s}}_{\mathrm{h}} &= \mathbf{U}\left(\hat{\theta}\right)^{\dagger}\mathbf{y}_{\mathrm{h}}. \end{aligned} \tag{21}$$

Then, between their relationship according to (4) and (5), we can retrieve the polarization parameters as

$$\begin{aligned} \hat{\gamma}_m &= \arctan\left(\sqrt{\left(\hat{s}_{\mathrm{e}k}\times\hat{s}^*_{\mathrm{e}k}\right)\Big/\left(\hat{s}_{\mathrm{h}k}\times\hat{s}^*_{\mathrm{h}k}\right)}\right), \\ \hat{\eta}_m &= \arg\left(\hat{s}_{\mathrm{e}k}/(\hat{s}_{\mathrm{h}k}\times\hat{\gamma}_m)\right). \end{aligned} \tag{22}$$

In the summary, the entire steps of the proposed P-ANM algorithm are shown in Algorithm 1.

Algorithm 1: The proposed P-ANM algorithm

Input:	The array geometry, the sampled signal vector $\mathbf{y}_{\mathrm{h}}$ and $\mathbf{y}_{\mathrm{e}}$, proper regularization parameter τ and Fourier expansion term number N ;
Step 1:	Calculate the mapping matrix $\mathbf{G}$ using (13) and (14) according to the array geometry;
Step 2:	Solve the SDP problem (18) by substituting $\mathbf{y}_{\mathrm{h}}$ and $\mathbf{y}_{\mathrm{e}}$ to obtain $\hat{\mathbf{c}}$ and then $\mathbf{h} = \tilde{\mathbf{G}}^{\mathrm{H}}\hat{\mathbf{c}}$;
Step 3:	Find the roots of the nonnegative polynomial (19) on the unit circle;
Step 4:	Recover the azimuth estimation $\hat{\theta}$ by (20) ;
Step 5:	Retrieval the pseudo signal amplitudes by (21) and then the polarization parameters $\hat{\gamma}$ and $\hat{\eta}$ by (22);
Output:	The azimuth estimation $\hat{\theta}$ and polarization estimation $\hat{\gamma}$, $\hat{\eta}$.

There are two notes here: 1) In the entire process, the main computational burden is solving the SDP problem. The complexity of the other processes can be relatively negligible. For the SDP problem (10), the complexity is $\mathbf{O}\left((M+1)^3\right)$. While for the SDP problems (16) and (18), the complexity is $\mathbf{O}\left((P+1)^3\right)$. Usually the P is larger than M, so we can see that the price of the virtual mapping is the increase of the arithmetic complexity.

2) In general, a two-dimensional line array can estimate both azimuth and elevation angles simultaneously. However, the two-dimensional UCA can only estimate the one-dimensional azimuth angle. The reason is that by using polar coordinates in (1), all the 360° azimuth range can be estimated, while only 180° azimuth range can be estimated by using line arrays. That is to say, compared with one-dimensional linear arrays, two-dimensional linear arrays utilize the added spatial dimension to obtain additional elevation angle estimation, while the UCA extends the range of azimuth angle estimation.

4. Simulations

In this section, the proposed P-ANM parameter estimation algorithm is verified using Monte Carlo simulations.

4.1 Feasibility Verification

Experiment 1: The simulation parameters are set as follows: The P-UCA with 40 COLD antennas pairs is arranged and its radius is set $r = 2\lambda$. Then $p = r$ for all the COLD antennas using the circular origin as the reference. Corresponding $N = 30$ is determined. For the signal parameters, assume there are three far-filed, narrowband and fully polarized signals with their azimuth θ, polarization angle γ and phase difference η combinations are $(-80°, 36°, 54°)$, $(10°, 45°, 144°)$ and $(70°, 54°, 324°)$, respectively. The complex amplitudes of the signals are generated randomly with the same modules and the signal-to-noise ratio is set SNR = 15 dB. Sampling the received signals of all the EMVS simultaneous as a single snapshot and performing 50 times Monte Carlo simulations, the results are shown in Fig. 4. As shown in the figures, the estimation results of all the azimuth and polarization parameters are around the true locations, indicating that the proposed P-ANM algorithm is effective and stable.

Experiment 2: In this experiment, the estimation ability of the proposed P-ANM algorithm around all the azimuths is verified. The three targets are moved around the 0° ∼ 360° circle with step 10°, and other parameters are kept the same with Experiment 1. In every azimuth, 5 times simulations are performed, the results are shown in Fig. 5. It can be seen that the azimuth and polarization parameters can be estimated successfully in all the 360° range, which indicates that the P-ANM algorithm has stable tracking ability.

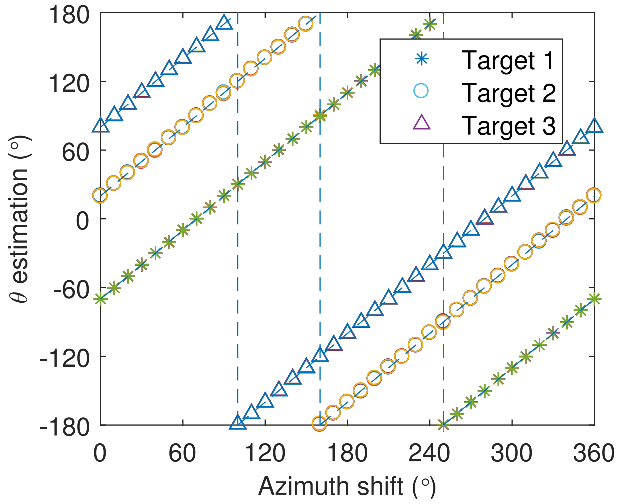

(a) The estimation results of θ

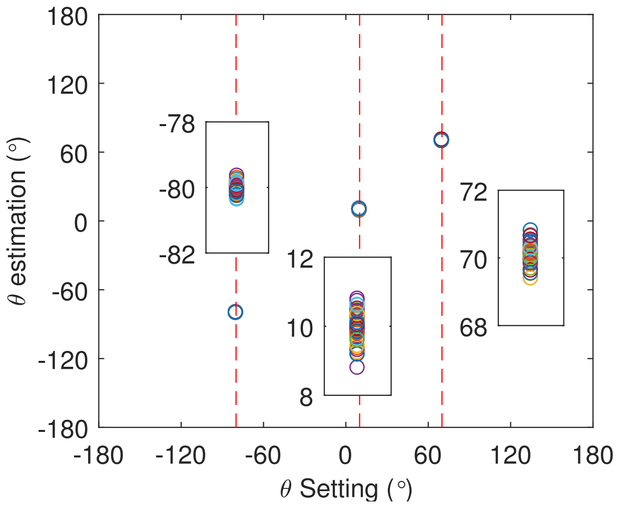

(a) The estimation results of θ

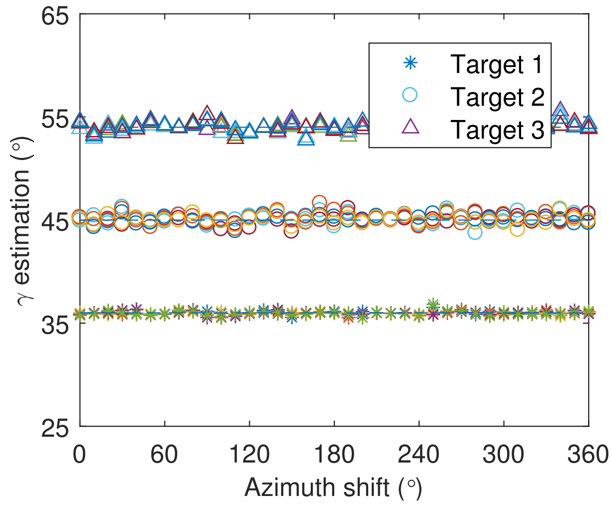

(b) The estimation results of γ

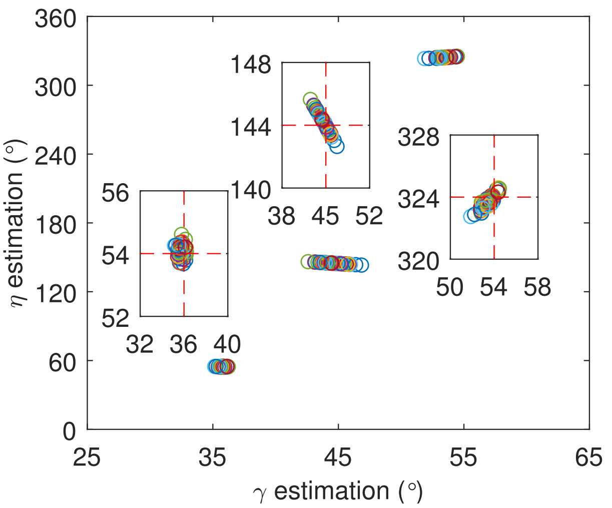

(b) The estimation results of γ and η

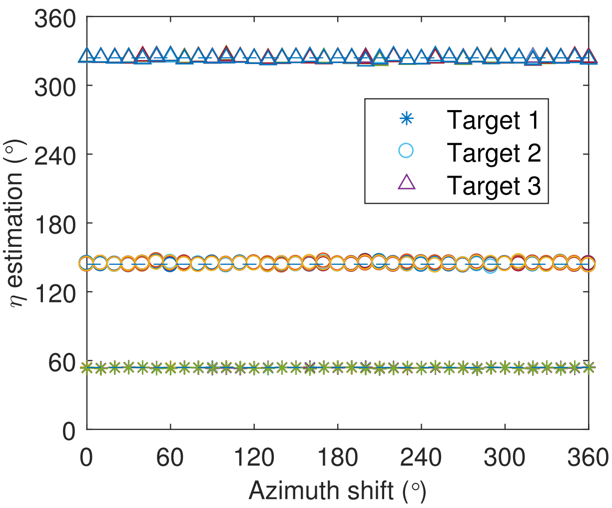

(c) The estimation results of η

Fig. 4. The estimation results.

Fig. 5. The estimation results with azimuth shift.

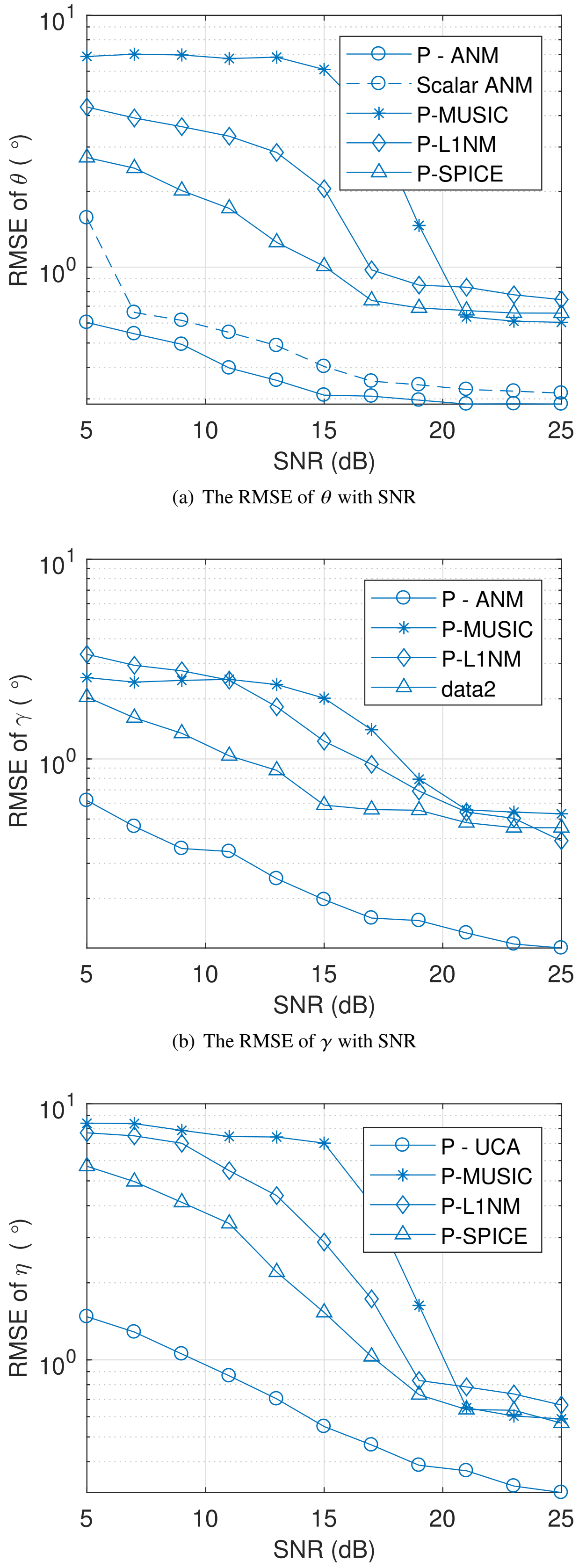

(a) The RMSE of θ with SNR

(b) The RMSE of γ with SNR

(c) The RMSE of η with SNR

Fig. 6. The estimation RMSE with SNR.

4.2 Estimation Performance

Experiment 3: In this experiment, the estimation accuracy of the proposed P-ANM algorithm is compared with polarization MUSIC (P-MUSIC), polarization L1NM (P-L1NM) and polarization SPICE (P-SPICE) algorithms. And for the azimuth parameter, the scalar ANM is also joined with the same signals from the scalar UCA array. The root mean square error (RMSE) of every parameter is used as the evaluation index, which is defined as

$$\mathrm{RMSE}_{\phi} = \sqrt{\frac{1}{K\times \mathrm{Iter}} \sum_{k=1}^{K} \sum_{i=1}^{\mathrm{Iter}} \left(\hat{\phi}_{ki} - \phi_k\right)^2} \tag{23}$$

where Iter is the number of Monte Carlo simulations, ϕ_k denotes the true value of θ_k, γ_k or η_k, and $\hat{\phi}_{ki}$ are corresponding estimation result of the ith Monte Carlo simulation. Total 500 times Monte Carlo simulations are run for each algorithm in each SNR and the results are counted in Fig. 6.

There are two notations here that: 1) the P-MUSIC and P-SPICE algorithms cannot work with only single snapshot. Therefore, they are performed with 20 snapshots here, while the P-ANM and P-L1NM algorithms are performed with only single snapshot. 2) only single snapshot is used for the estimation, so higher SNR is need compared with multiple snapshots, and the SNR variation is set 5 dB ∼ 25 dB. The simulation results show that the proposed P-ANM algorithm has excellent performance in all the SNR variations compared with the others.

Experiment 4: Finally, the resolution is verified. Two signals are set with the parameters $(10°, 30°, 120°)$, $(10° + \Delta, 60°, 240°)$, where the Δ is the azimuth spacing of the two signals and increased from $2°$ to $15°$ with step $1°$. The SNR is set 15 dB and 100 times Monte Carlo simulations are performed. If two signals are estimated and the total error is less than $5°$, this estimation was marked as a success. The success probability of all the algorithms are shown in Fig. 7. It shows that the proposed P-ANM algorithm has a high angular resolution compared with the others. If the threshold is reached, its estimated success probability can extremely increase.

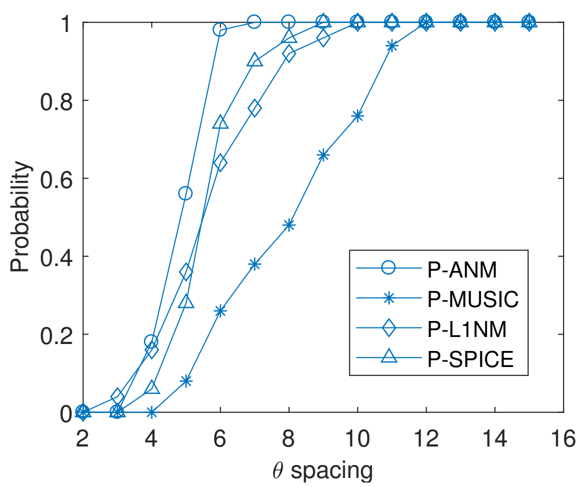

Fig. 7. The success probability with azimuth spacing.

5. Conclusion

In this paper, the novel P-ANM algorithm is proposed for joint azimuth and polarization estimation based on the P-UCA. The P-UCA model is converted into the virtual uniform array model to apply the P-ANM algorithm. The dual SDP problem is used to calculate the P-ANM formulate and the polynomial roots are searched for the parameter estimation. The simulations show the proposed P-ANM algorithm has good estimation performance with only single snapshot. It also has stable estimation performance within the range $0^\circ \sim 360^\circ$. And compared with other algorithms, it has lower RMSE for all the azimuth and polarization parameters and higher probability of successful estimation.

References

[1] PAN, B., DONG, L., YU, X., et al. Joint polarization-space-time processing for mainlobe jamming via CP decomposition. *IEEE Sensors Journal*, 2023, vol. 23, no. 13, p. 14781–14794. DOI: 10.1109/JSEN.2023.3279069

[2] ZHANG, Q., JIANG, H., LIU, Y. Joint range, angle and polarization estimation in polarimetric FDA-MIMO radar based on Tucker tensor decomposition. *EURASIP Journal on Advances in Signal Processing*, 2023, no. 1, p. 2023–2039. DOI: 10.1186/s13634-023-00997-8

[3] HU, Y., ZHAO, Y., CHEN, S., et al. Two-dimensional direction-of-arrival estimation method based on interpolation fitting for airborne conformal MIMO radar in a multipath environment. *Digital Signal Processing*, 2022, vol. 122, p. 1–13. DOI: 10.1016/j.dsp.2021.103374

[4] XU, Z., WU, J., XIONG, Z., et al. Low-angle tracking algorithm using polarisation sensitive array for very-high frequency radar. *IET Radar, Sonar and Navigation*, 2014, vol. 8, no. 9, p. 1035–1041. DOI: 10.1049/iet-rsn.2014.0041

[5] EBIHARA, S., KURODA, T., KORESAWA, Y., et al. Improved discrimination of subsurface targets using a polarization-sensitive directional borehole radar. *IEEE Transactions on Geoscience and Remote Sensing*, 2016, vol. 54, no. 11, p. 6429–6443. DOI: 10.1109/TGRS.2016.2585178

[6] BARAT, M., KARIMI, M., MASNADI-SHIRAZI, M. A. Direction of arrival estimation in vector-sensor arrays using higher-order statistics. *Multidimensional Systems and Signal Processing*, 2022, vol. 33, no. 1, p. 161–187. DOI: 10.1007/s11045-020-00734-z

[7] JAMSHIDPOUR, S., KARIMI, M., MASNADI-SHIRAZI, M. A. A coarray processing technique for nested vector-sensor arrays with improved resolution capabilities. *Digital Signal Processing*, 2022, vol. 130, p. 1–10. DOI: 10.1016/j.dsp.2022.103715

[8] ZHAO, W., MENG, X., CAO, B., et al. Efficient DOA-polarization estimation for 2-D mirrored array based on the hybrid aperture expansion. *Digital Signal Processing*, 2024, vol. 145, p. 1–13. DOI: 10.1016/j.dsp.2023.104344

[9] YANG, Y., JIANG, G. Efficient DOA and polarization estimation for dual-polarization synthetic nested arrays. *IEEE Systems Journal*, 2022, vol. 16, no. 4, p. 6277–6288. DOI: 10.1109/JSYST.2021.3134470

[10] MIRON, S., LE BIHAN, P., MARS, J. I. Quaternion-MUSIC for vector-sensor array processing. *IEEE Transactions on Signal Processing*, 2006, vol. 54, no. 4, p. 1218–1229. DOI: 10.1109/TSP.2006.870630

[11] LE BIHAN, N., MIRON, S. M., MARS, J. I. MUSIC algorithm for vector-sensors array using biquaternions. *IEEE Transactions on Signal Processing*, 2007, vol. 55, no. 9, p. 4773–4784. DOI: 10.1109/TSP.2007.896067

[12] LI, Y., ZHANG, J., HU, B., et al. A novel 2-D quaternion ESPRIT for joint DOA and polarization estimation with crossed-dipole. In *Proceedings of the IEEE International Conference on Acoustics, Speech and Signal Processing (ICASSP)*. Vancouver (Canada), 2022, p. 1038–1043. DOI: 10.1109/ICASSP43922.2022.9746221

[13] QU, Y., LU, J., ZHAO, X., et al. Augmented tensor MUSIC for DOA estimation using nested acoustic vector-sensor array. *IEEE Signal Processing Letters*, 2022, vol. 29, p. 1624–1628. DOI: 10.1109/LSP.2022.3191254

[14] LOU, M., QU, X., WANG, Z., et al. Augmented quaternion ESPRIT-type DOA estimation with a crossed-dipole array. *IEEE Transactions on Signal Processing*, 2023, vol. 61, p. 1–14. DOI: 10.1109/TGRS.2023.3274182

[15] CHEN, H., WANG, W., LIU, W. Augmented quaternion ESPRIT for DOA estimation with polarization-sensitive arrays. *IEEE Transactions on Signal Processing*, 2022, vol. 29, p. 548–552. DOI: 10.1109/LSP.2019.2962463

[16] MALIOUTOV, D., CETIN, M., WILLSKY, A. S. A sparse signal reconstruction perspective for source localization with sensor arrays. *IEEE Transactions on Signal Processing*, 2005, vol. 53, no. 8, p. 3010–3022. DOI: 10.1109/TSP.2005.850882

[17] WEI, Z., LI, X., WANG, W., et al. An efficient super-resolution DOA estimator based on grid learning. *Radioengineering*, 2019, vol. 28, no. 4, p. 785–792. DOI: 10.13164/re.2019.0785

[18] RAJ, A. G., MCCLELLAN, J. H. Single coarray snapshot super-resolution DOA estimation using sparse Bayesian learning. *IEEE Transactions on Signal Processing*, 2019, vol. 26, no. 1, p. 119–123. DOI: 10.1109/LSP.2019.2962463

[19] TIAN, Y., SUN, X., ZHAO, S. Sparse-reconstruction-based direction of arrival, polarisation and power estimation using a cross-dipole array. *IET Radar Sonar and Navigation*, 2015, vol. 9, no. 6, p. 727–731. DOI: 10.1049/iet-rsn.2013.0169

[20] DAS, A. A Bayesian sparse-plus-low-rank matrix decomposition approach for direction-of-arrival estimation. *IEEE Sensors Journal*, 2017, vol. 17, no. 15, p. 4894–4902. DOI: 10.1109/JSEN.2017.2715347

[21] CHANG, W., RU, J., DENG, L. Stokes parameters and DOA estimation of polarised sources with an unknown number of sources. *IET Radar Sonar and Navigation*, 2018, vol. 12, no. 6, p. 218–226. DOI: 10.1049/iet-rsn.2013.0415

[22] SHI, S., LI, Y., YANG, D., et al. Sparse representation-based direction-of-arrival estimation using circular acoustic vector sensor arrays. *Digital Signal Processing*, 2020, vol. 99, p. 1–17. DOI: 10.1016/j.dsp.2020.102675

[23] CHANDRASEKARAN, V., RECHT, B., PARRILO, P. A., er al. The convex geometry of linear inverse problems. *Foundations of Computational Mathematics*, 2012, vol. 12, no. 6, p. 805–849. DOI: 10.1007/s10208-012-9135-7

[24] BHASKAR, B. N., TANG, G., RECHT, B. Atomic norm denoising with applications to line spectral estimation. *IEEE Transactions on Signal Processing*, 2013, vol. 61, no. 23, p. 5987–5999. DOI: 10.1109/TSP.2013.2273443

[25] CHI, Y., CHEN, Y. Compressive two-dimensional harmonic retrieval via atomic norm minimization. *IEEE Transactions on Signal Processing*, 2015, vol. 63, no. 4, p. 1030–1042. DOI: 10.1109/TSP.2014.2386283

[26] CHEN, P., CHEN, Y., CAO, J., et al. A new atomic norm for DOA estimation with gain-phase errors. *IEEE Transactions on Signal Processing*, 2020, vol. 68, p. 4293–4306. DOI: 10.1109/TSP.2020.3010749

[27] GONG, Q., REN, S., ZHONG, S., et al. DOA estimation using a sparse array with gain-phase error based on a novel atomic norm. *Digital Signal Processing*, 2022, vol. 120, p. 1–14. DOI: 10.1016/j.dsp.2021.103266

[28] TENG, L., WANG, Q., CHEN, H., et al. Atomic norm-based DOA estimation with sum and difference co-arrays in coexistence of circular and non-circular signals. *Circuits Systems and Signal Processing*, 2021, vol. 40, no. 10, p. 4293–5053. DOI: 10.1007/s10208-021-01708-7

[29] CHEN, H., WANG, W. L., LIU, W., et al. Derivative ESPRIT for DOA and polarization estimation for UCA using tangential individually-polarized dipoles. *Digital Signal Processing*, 2020, vol. 96, p. 1–10. DOI: 10.1016/j.dsp.2020.102599

[30] ZHANG, Y., WONG, K. The "Co-centered orthogonal loop/dipole" (COLD) array's "Spatial matched filter" beam-steering. *IEEE Transactions on Aerospace and Electronic Systems*, 2022, vol. 58, no. 6, p. 5932–5936. DOI: 10.1109/TAES.2022.3171749

[31] CHEN, H., WANG, W. L., LIU, W., et al. An exact near-field model-based localization for bistatic MIMO radar with COLD arrays. *IEEE Transactions on Vehicular Technology*, 2023, vol. 69, no. 12, p. 16021–16030. DOI: 10.1109/TVT.2023.3294625

[32] YIN, K., DAI, Y., GAO, C. Near-field DOA-range and polarization estimation based on exact propagation model with COLD arrays. *Circuits Systems and Signal Processing*, 2022, vol. 41, p. 5183–5200. DOI: 10.1007/s10208-022-02029-z

[33] NEHORAI, A., PALDI, E. Vector-sensor array processing for direction-of-arrival estimation and source polarization. *IEEE Transactions on Signal Processing*, 1994, vol. 42, no. 2, p. 376–398. DOI: 10.1109/78.275610

[34] LI, J., STOICA, P., ZHENG, D. Efficient direction and polarization estimation with a COLD array. *IEEE Transactions on Antennas and Propagation*, 1996, vol. 42, no. 2, p. 539–547. DOI: 10.1109/78.489306

[35] WEN, F., SHI, J., ZHANG, Z. Joint 2D-DOD, 2D-DOA and polarization angles estimation for bistatic EMVS-MIMO radar via PARAFAC analysis. *IEEE Transactions on Vehicular Technology*, 2019, vol. 69, no. 2, p. 1626–1637. DOI: 10.1109/TVT.2023.2957511

[36] DONOHO, D. L. Compressed sensing. *IEEE Transactions on Information Theory*, 2006, vol. 52, no. 4, p. 1289–1306. DOI: 10.1109/TIT.2006.871582

[37] CANDES, E. J., FERNANDEZ-GRANDA, C. Towards a mathematical theory of super-resolution. *Communications on Pure and Applied Mathematics*, 2014, vol. 67, no. 6, p. 906–956. DOI: 10.1002/cpa.21455

[38] XENAKI, A., GERSTOFT, P. Grid-free compressive beamforming. *Journal of the Acoustical Society of America*, 2015, vol. 137, no. 4, p. 1923–1935. DOI: 10.1121/1.4916269

About the Authors . . .

Tao YU was born in Qinhuangdao, China. He received his B.A. degree from Harbin Engineering University in 2012. He is currently pursuing his Ph.D. degree for Information and Communication Engineering in Harbin Engineering University. His research interests include the array signal processing.

Lutao LIU (corresponding author) was born in Harbin, China. He received the B.A. degree in Electrical Engineering from Southeast University, Nanjing, China, in 2000, the M.Sc. degree in Telecommunication Engineering from the Harbin Institute of Technology, Harbin, China in 2003, the M.Sc. degree in Microelectronics from the Delft University of Technology, Delft, The Netherlands, in 2005, and the Ph.D. degree in Telecommunication Engineering from Harbin Engineering University, Harbin, in 2011. He was a Visiting Scholar with Signal Processing and Communication (SPAC) Laboratory, Stevens Institute of Technology, Hoboken, NJ, USA, in 2013. He is currently an Associate Professor with the College of Information and Communication, Harbin Engineering University. His research interests include the general area of signal processing for telecommunication.